Available online at www.sciencedirect.com
ScienceDirect
Trans. Nonferrous Met. Soc. China 25(2015) 1822−1830
Transactions of Nonferrous Metals Society of China
www.tnmsc.cn

Hot deformation behavior and workability of pre-extruded ZK60A magnesium alloy

Shi-yi WANG[1], Lei GAO[2], Alan A. LUO[3], De-jiang LI[1], Xiao-qin ZENG[1]

1. National Engineering Research Center of Light Alloy Net Forming, Shanghai Jiao Tong University, Shanghai 200240, China;
2. General Motors China Science Lab, Shanghai 201206, China;
3. College of Engineering, the Ohio State University, Columbus, OH 43210, USA

Received 5 August 2014; accepted 10 December 2014

Abstract: The hot deformation behavior and workability of pre-extruded ZK60A magnesium alloy were investigated by compression tests in the temperature range of 250−450 °C and the strain rate range of 0.001−10 s^{-1}. The constitutive equation for the pre-extruded ZK60A alloy can be described by hyperbolic sine function. Processing maps were constructed from true strains of −0.2 to −0.8. The alloy experienced complete dynamic recrystallization (DRX) and showed good workability in the temperature range of 300−400 °C and the strain rate range of 0.01−0.001 s^{-1}, where hot working in pre-extruded ZK60A, such as forging, can be carried out. For large deformation to true strain of over −0.5, strain rates above 0.1 s^{-1} are not recommended at all temperatures, where flow instability such as local strain concentration, twinning deformation, abnormal grain growth, micro-cracks, and shear fracture were observed. Climb-controlled dislocation creep dominates both the plastic deformation and nucleation of DRX of the pre-extruded ZK60A magnesium alloy.

Key words: pre-extruded ZK60A magnesium alloy; hot deformation; processing map; constitutive equation; workability

1 Introduction

Wrought magnesium alloys are receiving increasing attention due to their higher strength and ductility compared with castings. In the automotive industry, for example, magnesium forgings are considered as potential lightweight alternatives to some steel and aluminum components, such as road wheel, control arm and knuckle [1,2]. However, since magnesium has hexagonal close-packed structure, magnesium alloys normally exhibit low formability near room temperature. In order to obtain the adequate ductility required for plastic forming, magnesium alloys need to be deformed above 200 °C, where non-basal slips can be activated to enhance hot workability [3,4].

ZK60 magnesium alloy (Mg−6.0Zn−0.6Zr, mass fraction, %) in T5 condition has the best combination of strength and ductility at room temperature of commercial wrought magnesium alloys [5]. Forgings in ZK60 alloy find applications in high strength parts for satellites, helicopter gearboxes and rotor hubs, bicycles frames, road wheels, missile frames and interstage fairings, brake housings and landing gear struts [5]. Therefore, it is important to explore the hot deformation behavior of ZK60 magnesium alloy, especially at strain rates over 1.0 s^{-1} for reasonable productivity. GALIYEV et al [6], McQUEEN et al [7] and WANG et al [8] investigated the hot deformation mechanism and workability of ZK60 alloys. Unfortunately, most studies are limited to ZK60 castings, which inherently have poor formability because of inhomogeneous coarse grains and porosity in the microstructure.

Pre-extruded ZK60A alloy (normally used for forging billets for better formability) after homogenization treatment was investigated in this work. The aim of the present investigation was to study the hot deformation behavior and workability of pr-extruded ZK60A magnesium alloy to explore its potential for automotive applications. The effects of strain, strain rate, and temperature on the deformation mechanisms and dynamic recrystallization (DRX) behavior of this alloy were investigated.

Foundation item: Projects (51171113, 51301107) supported by the National Natural Science Foundation of China
Corresponding author: Xiao-qin ZENG; Tel: +86-21-54742301; E-mail: xqzeng@sjtu.edu.cn
DOI: 10.1016/S1003-6326(15)63788-8

2 Experimental

Pre-extruded ZK60A alloy billets of 75 mm in diameter obtained from Magnesium Elektron North America were used as the initial material in this work. The actual chemical composition of the alloy billets was determined by using inductively coupled plasma atomic emission spectroscopy (ICP-AES), and is listed in Table 1.

Table 1 Chemical composition of pre-extruded ZK60A magnesium alloy (mass fraction, %)

Zn	Zr	Al	Fe	Ni	Cu	Mn	Mg
4.88	0.58	<0.01	<0.01	<0.01	<0.005	<0.005	Bal.

The billets were firstly homogenized at 400 °C for 24 h. Cylindrical specimens of 10 mm in diameter and 15 mm in height were machined from the homogenized billets with their longitudinal axis parallel to the pre-extrusion direction. Uniaxial compression tests were carried out using a DSI Gleeble−3500 system at the temperature between 250 °C and 450 °C with an increment of 50 °C, and at a constant strain rate of 0.001, 0.01, 0.1, 1.0 and 10 s^{-1}, respectively.

The specimens were heated to a preset temperature at a heating rate of 2 °C/s and soaked for 3 min in a low vacuum to allow the temperature to equalize throughout the specimens. Graphite flakes were used as the lubricant to minimize the friction between the indenter and the specimen. The specimens were then deformed up to true strains (ε) of −0.1 to −1.0 (height reduction of ~10% to ~63%) and rapidly quenched into water within 5 s. The true stress−strain (σ_T−ε_T) curves were derived from the nominal stress−strain (σ_N−ε_N) curves obtained in compression according to the following formulas: $\sigma_T=\sigma_N(1+\varepsilon_N)$, $\varepsilon_T=\ln(1+\varepsilon_N)$.

For metallographic examination, the initial and deformed specimens were sectioned parallel to the compression axis and the cut surfaces were prepared for microstructure observation at the center of these sections. Microstructures were observed by optical microscopy (OM) and scanning electron microscopy (SEM). Samples were etched with a solution of 150 mL water, 1 g oxalic acid, 1 mL nitric acid, and 1 mL acetic acid for 10−15 s. The microscopy was constrained to the central part of the section parallel to the compressive direction. The average grain size (d) was determined using the mean linear intercept method, where d=1.74L, L is the linear intercept size.

3 Results and discussion

3.1 Initial microstructure

Figure 1 shows the as-received and homogenized microstructures of the pre-extruded ZK60A alloy. The as-received microstructure (Fig. 1(a)) consists of equiaxed grains of ~14 μm and coarse elongated grains

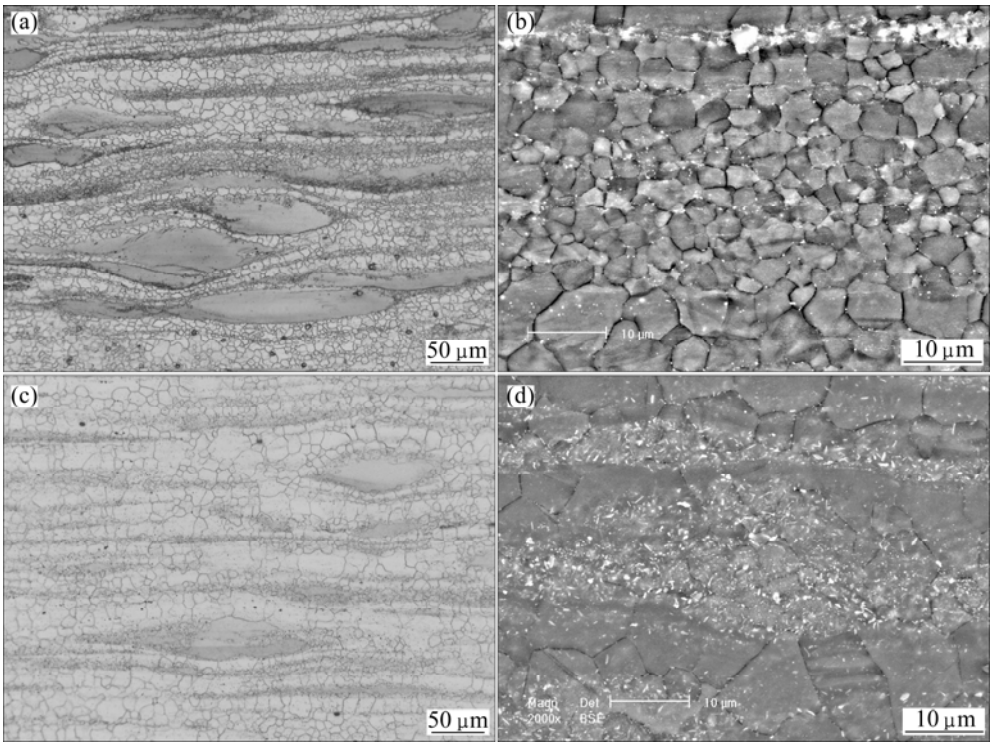

Fig. 1 Optical (a, c) and SEM (b, d) images showing as-received (a, b) and homogenized (c, d) microstructures of pre-extruded ZK60A alloy (Extrusion direction is horizontal)

along the extruded bands, which increases material inhomogeneity. Many second phases (the white particles in Fig. 1(b)) of 100−150 nm formed stringers in the extrusion direction. Single particles along the grain boundaries or inside the grains were also observed. These phase particles contain Zr-rich cores within the grains, Zn-rich rings at the grain boundaries, some Mg−Zn eutectic constituents and the Zn−Zr intermetallics [9−11]. No significant grain growth but less extruded bands was observed in the homogenized microstructure (Fig. 1(c)). The second phase particles scattered in the matrix, as shown in Fig. 1(d).

3.2 Flow behavior

Figure 2 shows the true stress−true strain curves of the pre-extruded ZK60A alloy compressed at different strain rates and different temperatures. In almost all cases, the curves reveal initial work hardening until a peak stress is attained at a true strain of less than −0.2 and then decreases to finally attain a steady state at a true strain of approximately −0.5. This subsequent decrease or softening in the flow stress is typical for materials undergoing DRX [6], rather than dynamic recovery due to the low stacking-fault energy (SFE) 60−78 mJ/m^2 of magnesium [12]. Evidence for the occurrence of DRX

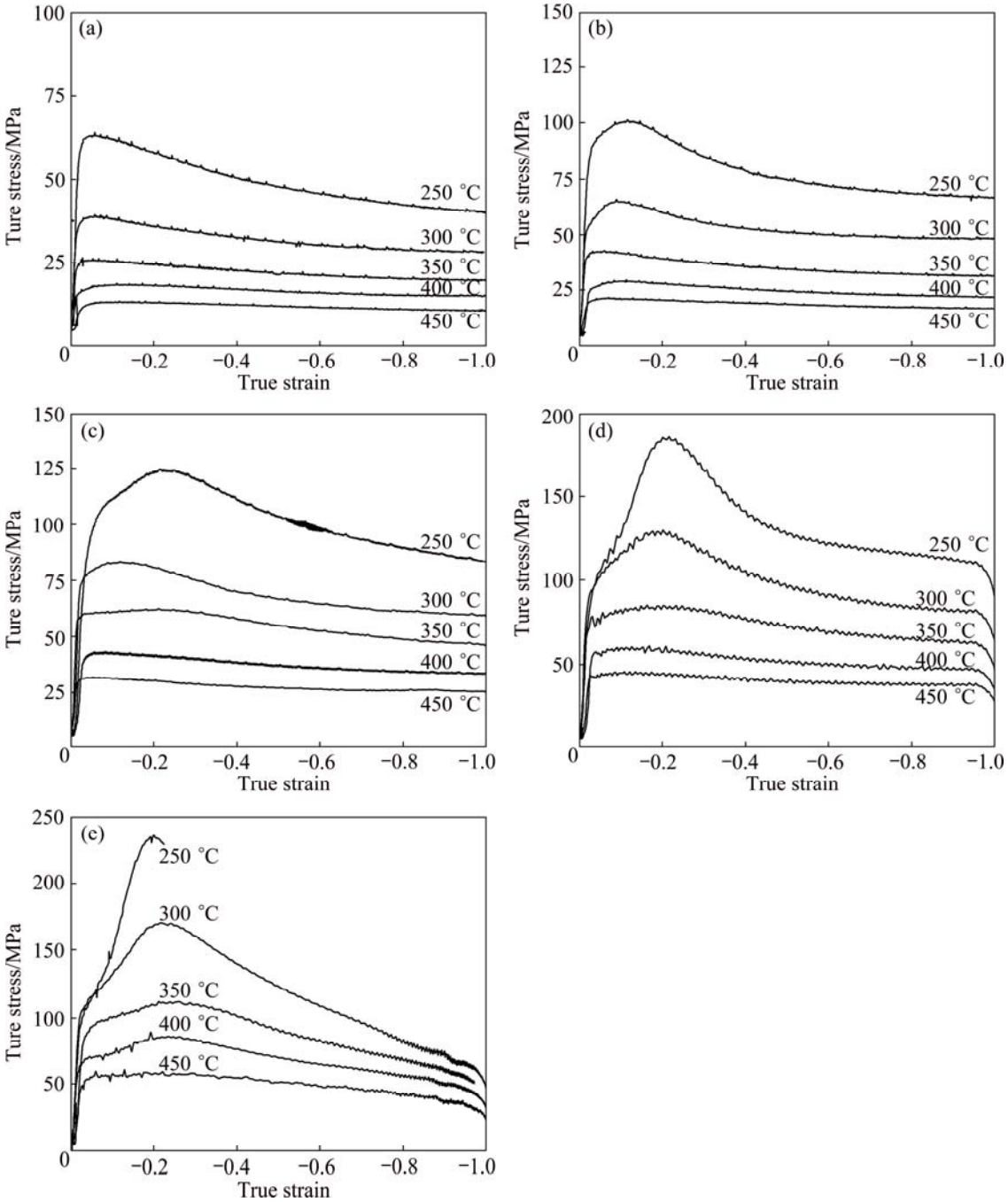

Fig. 2 Typical true stress−true strain curves obtained at different temperatures: (a) $\dot{\varepsilon}$=0.001 s^{-1}; (b) $\dot{\varepsilon}$ = 0.01 s^{-1}; (c) $\dot{\varepsilon}$ = 0.1 s^{-1}; (d) $\dot{\varepsilon}$ = 1.0 s^{-1}; (e) $\dot{\varepsilon}$ = 10 s^{-1}

will be presented in more detail below.

In comparison to the alloys fabricated by chill casting [6] and squeeze casting [8], pre-extruded ZK60A alloy exhibits lower flow stresses, which is partly due to its fine microstructure. The lower stress resistance to hot deformation or better forgeability allows forging operation to be performed at lower temperatures, which is overall beneficial. It should be noted that the abrupt failure was observed at the highest strain rate of 10 s^{-1} and at the lowest temperature of 250 °C (Fig. 2(e)). A very rapid decline from a peak instead of the expected steady flow was observed by increasing the temperature from 250 °C to 450 °C, which is partly due to crack propagation [7]. The following processing maps and microstructures of the pre-extruded ZK60A magnesium alloy will subsequently support this type of flow instabilities.

3.3 Constitutive equations and hot deformation mechanism

As shown in Fig. 2, the peak stress (σ_p) decreases with increasing deformation temperature (T) and increases with increasing strain rate ($\dot{\varepsilon}$). The hyperbolic-sine equation, proposed by SELLARS and MCTEGART [13] and GAROFALO [14], is widely employed to describe the relationship between the deformation parameters for wide range of stresses [15]. Therefore, σ_p was subjected to constitutive analysis for T and $\dot{\varepsilon}$ dependence according to [15,16]:

$$Z = \dot{\varepsilon}\exp(\frac{Q}{RT}) = A[\sinh(\alpha\sigma_p)]^n \quad (1)$$

where Z is Zener−Hollomon parameter which is the temperature-compensated strain rate, A (s^{-1}) and α (MPa^{-1}) are material constants independent of temperature, n is the stress exponent, Q is the activation energy, and R = 8.31 J/(K·mol).

At constant deformation temperature and assuming that the activation energy is constant, partial differentiation of Eq. (1) yields [17]

$$n = \left\{\frac{\partial \ln\dot{\varepsilon}}{\partial \ln[\sinh(\alpha\sigma_p)]}\right\}_T \quad (2)$$

The relationship between $\ln\dot{\varepsilon}$ and $\ln[\sinh(\alpha\sigma_p)]$ is shown in Fig. 3(a) for all temperatures. The adjustable stress multiplier α is found to produce parallel lines in a plot of $\ln\dot{\varepsilon}$ versus $\ln[\sinh(\alpha\sigma_p)]$ at a value of 0.01 MPa^{-1}.

At constant strain rate, partial differentiation of Eq. (1) yields [17]

$$Q = Rn\left\{\frac{\partial \ln[\sinh(\alpha\sigma_p)]}{\partial(1/T)}\right\}_{\dot{\varepsilon}} \quad (3)$$

The plot of $\ln[\sinh(\alpha\sigma_p)]$ versus $1/T$ is shown in Fig. 3(b) for all strain rates. The liner regression of these data results in average values of 5.33 and 149 kJ/mol for n and Q, respectively.

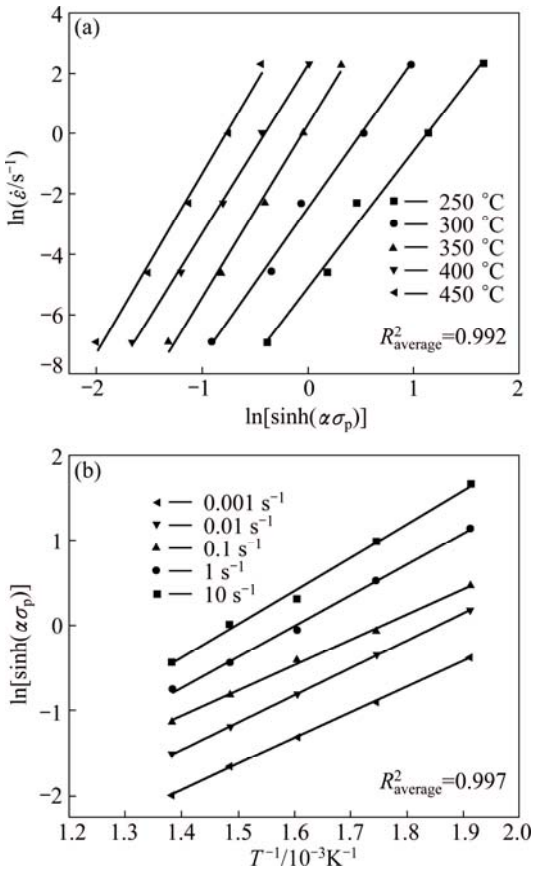

Fig. 3 Variation in $\ln\dot{\varepsilon}$ as a function of $\ln[\sinh(\alpha\sigma_p)]$ at various temperatures (a) and variation in $\ln[\sinh(\alpha\sigma_p)]$ as a function of $1/T$ at various strain rates (b)

One of the deformation mechanisms potentially activated under the investigated process conditions is dislocation creep [18], which includes conservative and non-conservative motion of dislocation. The former is known as solute drag creep with n = 3.3, while the latter is termed dislocation climb creep with n = 5−7 [18,19]. Therefore, the n value of approximately 5 suggests that the climb-controlled dislocation creep is the hot deformation mechanism for the present pre-extruded ZK60A alloy.

The apparent activation energy Q value of 149 kJ/mol for the pre-extruded ZK60A alloy is close to but slightly higher than 130−140 kJ/mol for magnesium volume self-diffusion [20,21] and 134 kJ/mol for as-cast ZK60 ingots in hot torsion testing [7] and 110 kJ/mol for semi-continuous cast alloy ZK60 high strain rate deformation [22]. The slightly higher value of activation energy of the present alloy is probably due to the presence of the fine precipitates (Fig. 1), which can hinder dislocation movement during deformation. This

results in more energy for dislocation cross slip and climb, consequently high activation energy for the pre-extruded ZK60A alloy. A similar role of secondary phase was also reported in other magnesium alloys [3,23,24].

Based on the stress exponent and activation energy, the dominant deformation mechanism in the pre-extruded ZK60A alloy under the deformation conditions of the present work is diffusion controlled and likely accompanied by climb-controlled dislocation creep [6,18]. This is similar to that for the chill cast and solution-treated ZK60 alloy [6].

According to Eq. (1), the plot of ln Z vs ln[sinh($\alpha\sigma_p$)] can be used to find the relationship between Z and σ_p. The corresponding curve is shown in Fig. 4 and the resultant equation with new regression constants is as follows:

$$\dot{\varepsilon} = 2.76 \times 10^{12}[\sinh(0.01\sigma_p)] \cdot 5.28\exp(-\frac{148527.642}{8.31T}) \quad (4)$$

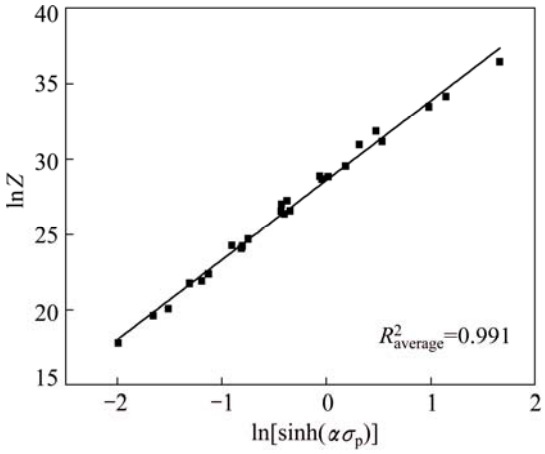

Fig. 4 Relationship between Zener−Hollomon parameter and ln[sinh($\alpha\sigma_p$)] in pre-extruded ZK60A alloy

Figure 5 shows the relationship between the calculated flow stress using Eq. (4) and the experimental flow stress of the pre-extruded ZK60A alloy. It is obvious that hyperbolic sine constitutive equation can well describe (with a correlation coefficient R^2= 0.99) the flow behavior of climb-controlled dislocation creep in the pre-extruded ZK60A alloy.

3.4 Processing maps

A superimposition of the instability map on the power dissipation map constitutes a processing map, which is developed from the well-known dynamic materials model [25], where the workpiece undergoing hot deformation is considered to be a dissipater of power. The efficiency of power dissipation, η, is given by [26]

$$\eta = \frac{2m}{m+1} \quad (5)$$

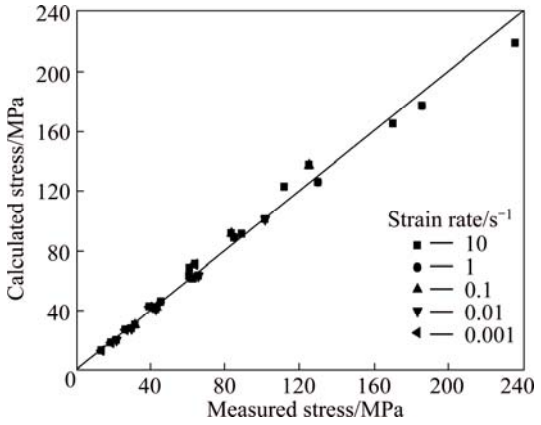

Fig. 5 Comparison of calculated and measured peak stress

where m is the strain rate sensitivity. The power dissipation map is obtained by plotting iso-efficiency contours of the parameter η in a temperature−strain rate frame at a constant strain. According to the continuum instability criterion [14,27], flow instability will occur during hot deformation if

$$\xi(\dot{\varepsilon}) = \frac{\partial \ln(m/(m+1))}{\partial \ln \dot{\varepsilon}} + m \le 0 \quad (6)$$

where $\xi(\dot{\varepsilon})$ is the instability parameter.

The variation of instability parameter with deformation temperature and strain rate constitutes an instability map which delineates regimes of instability where $\xi(\dot{\varepsilon})$ is negative. The processing map technique has been used earlier to study the hot deformation mechanisms in pure Mg [28] and AZ80 (Mg−8Al−0.5Zn) alloy [4].

Figure 6 shows the processing maps of pre-extruded ZK60A alloy obtained at true strains of −0.2, −0.3, −0.5 and −0.8, respectively. The efficiency of power dissipation is marked against each contour and the shadow regions correspond to the flow instability areas.

At a strain of −0.2 (Fig. 6(a)), the map exhibits a single domain in the temperature range of 300−400 °C and in the strain rate range of 0.01−0.001 with a peak efficiency of 35% occurring at 350 °C and 0.001 s^{-1}. As the strain is increased to −0.3 (Fig. 6(b)), this domain is retained and no obvious change is observed in the power dissipation map. Further increasing the strain to −0.5 (Fig. 6(c)) and −0.8 (Fig. 6(d)), this domain evolves into two separate domains, with one peak efficiency of 37% at 300 °C and 0.001 s^{-1} and the other peak of 31% at 450 °C and 0.01 s^{-1}.

Regarding Figs. 6(a)−(c), pre-extruded ZK60A alloy exhibits flow instability at lower temperatures (<300 °C) and strain rates over 1.0 s^{-1} at the beginning of the plastic deformation. Typically, flow instability occurs around the deformation condition of 250 °C and 10 s^{-1},

where premature failure of the material was observed in Fig. 2(e). Further deformation to strains up to −0.8 (Fig. 6(d)) results in flow-instability at strain rates over 0.1 s^{-1} and at all of the investigated temperatures.

3.5 Microstructural evolution

Figure 7 shows the microstructures obtained for the specimens deformed at 0.001 s^{-1} and 350, 300, and 250 °C, respectively. The former two correspond to the

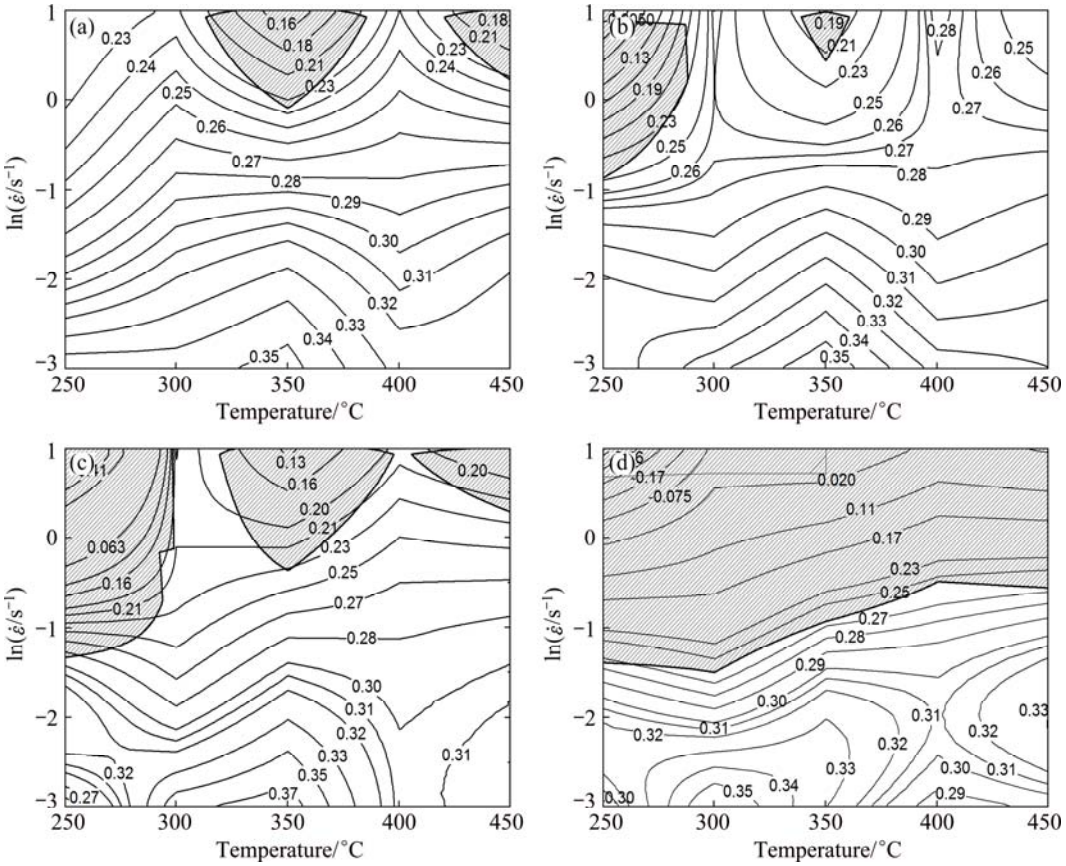

Fig. 6 Processing maps of ZK60A magnesium alloy at different true strains: (a) ε =−0.2; (b) ε= −0.3; (c) ε= −0.5; (d) ε=−0.8

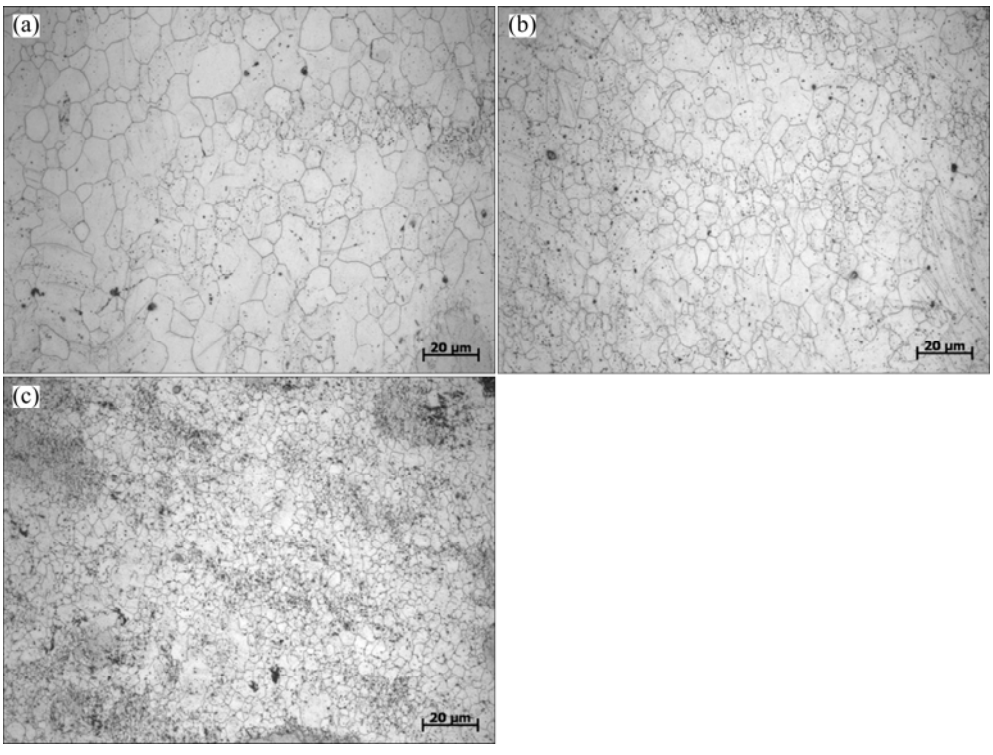

Fig. 7 Optical microstructures of specimens after compression to true strain of −1.0 at 0.001 s^{-1}: (a) 350 °C; (b) 300 °C ; (c) 250 °C

peak power dissipation efficiency in the processing maps, while the later also exhibits high power dissipation efficiency of ~31% (Fig. 6(d)). Complete DRX grains in equiaxed shape with average grain sizes of approximately 16 μm, 13 μm, and 6 μm are observed, respectively. The size of the DRXed grains decreases with increasing the value of the Z parameter, i.e., the dislocation density in the deformed sample [29]. Align with the processing maps, the results suggest that the optimum processing window for the pre-extruded ZK60A alloy lies in the temperature range of 300−400 °C and the strain rate range of 0.01−0.001 s^{-1}.

Increasing the strain rate to 0.1 s^{-1}, the specimen deformed at 350 °C exhibits a non-uniform microstructure with incomplete DRX (shown in Fig. 8) due to the low efficiency of power dissipation of ~25% (Fig. 6(d)).

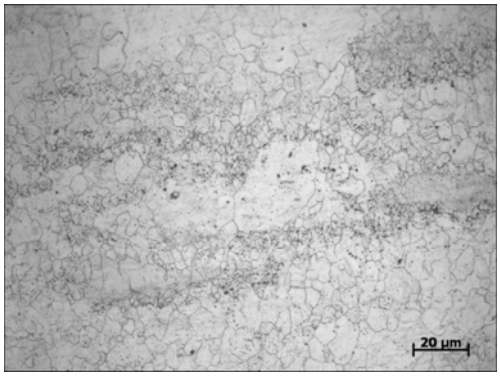

Fig. 8 Optical microstructure of specimen after compression to true strain of −1.0 at 350 °C and 0.1 s^{-1}

Figure 9 shows the microstructures of the specimen deformed at 450 °C and 10 s^{-1}, corresponding to the regime of flow instability in the processing maps (Fig. 6). Micro-cracks along the grain boundaries (indicated by the black arrows in Fig. 9(a)) are detected in the matrix, which are not desirable and detrimental to the final products. DRX is also observed in the microstructure, but is incomplete. This results in the fact that the steady state of the flow curves (Fig. 2(e)) is not able to be obtained during the hot deformation processing at high strain rate of 10 s^{-1}.

Abnormally large grains of over 100 μm have been observed at the very early deformation (Fig. 9(b)) and are retained after forming at elevated temperature (Fig. 9(c)). Boundaries of the abnormal coarse grains are corrugated and smaller grains (denoted by the arrows in Fig. 9(b)) are observed in the grain interiors. The small islands of the survived original structure may be characterized by a higher local density of the particles [30]. In fact, abnormal grain growth occurs during the heating and holding period of approximately 5 min. Therefore, hot working of the pre-extruded ZK60A alloy at 450 °C is not recommended.

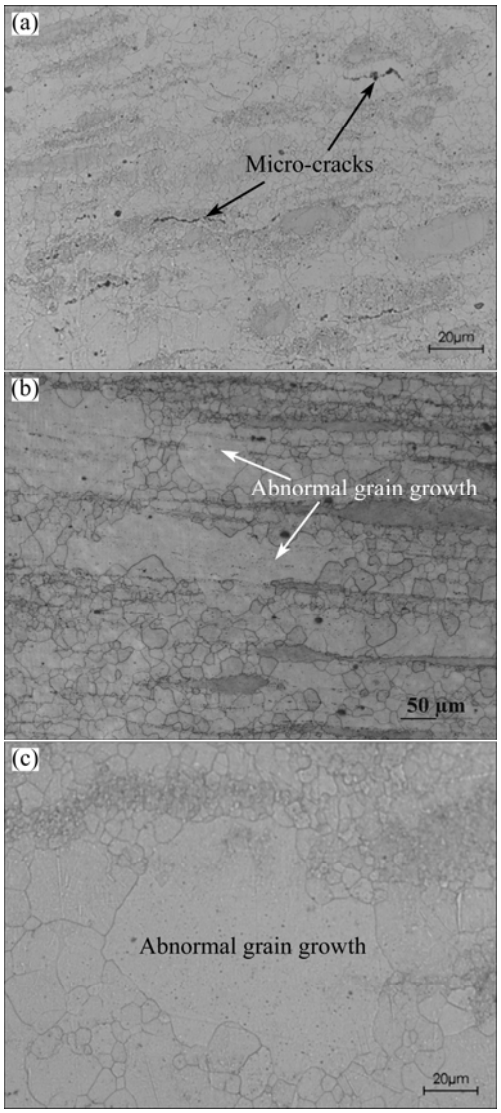

Fig. 9 Optical microstructures of specimens after compression to true strain of −1.0 (a,c) and −0.1 (b) at 450 °C and 10 s^{-1}

Figure 10 shows the microstructure of the specimen deformed at 250 °C and 10 s^{-1} to a true strain of about −0.2. Micro-cracks emerged at the grain boundaries due to the large stress concentration. This subsequently leads to the failure of the sample with continuous deformation. Deformation twinning is occasionally observed inside the large grains, and is believed to dominate the "concave" work hardening behavior in Fig. 2(e) [31]. This is not evident in tests carried out at higher temperatures and lower strain rates, where the flow curves are dominated by slip [32]. Both micro-cracks and deformation twinning result in the flow instability regime in the processing maps (Fig. 6). Almost complete DRX is observed, while the power dissipation efficiency is only about 22%. Compared to the incomplete DRX formed at the strain of −1.0, 450 °C and 10 s^{-1} (Fig. 9(a)), this effect is attributed to the decreased temperature, which is

accompanied by both an increase in dislocation density and a reduction in the fraction of mobile dislocation [33]. Boundaries of the DRX grains are not clear (Fig. 10(b)), suggesting that it might be low angle grain boundaries (LAGBs), which will develop as high angle grain boundaries (HAGBs) in case of continuous compression or annealing. DRX is also observed at twinning in the initial coarse grains.

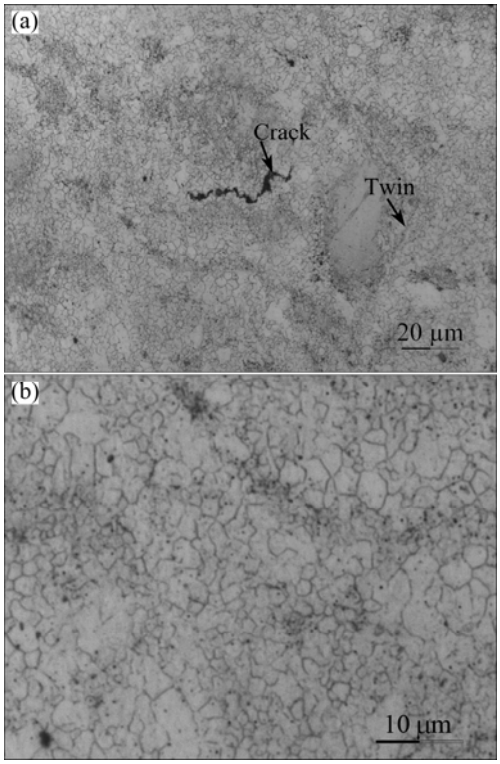

Fig. 10 Optical microstructures of specimen after compression to true strain of −0.2 at 250 °C and 10 s^{-1}: (a) Crack and twin; (b) DRX grains

4 Conclusions

1) The constitutive analysis showed that the hot deformation behavior of the pre-extruded ZK60A alloy satisfied the hyperbolic sine constitutive equation with a stress multiplier α value of 0.01 MPa^{-1}. The linear relation of the flow stress at the peak strain with Z value was obtained showing a stress exponent n of 5.28.

2) The processing maps exhibited a single domain of complete dynamic recrystallization in the range of 300−400 °C and 0.001−0.01 s^{-1}. It is recommended that the plastic forming in the pre-extruded ZK60A alloy, such as forging, would be performed at the above process window where the climb-controlled dislocation creep dominated both the plastic deformation and nucleation of DRX.

3) For large deformation to true strain of over −0.5, strain rates above 0.1 s^{-1} are not recommended at all temperatures, where flow instability such as local strain concentration, twinning deformation, abnormal grain growth, micro-cracks, and shear fracture were observed.

Acknowledgements

The authors would like to thank Magnesium Elektron North America for providing the materials.

References

[1] LUO A A. Wrought magnesium alloys and manufacturing processes for automotive applications [J]. SAE Technical Paper, 2005−01−0734.

[2] FUJITA M, YAMAMOTO Y, SAKATE N, HIRAHARA S, Development of magnesium forged wheel [J]. JSAE Rev, 1995, 16: 106−107.

[3] GAO Lei, LUO A A. Hot deformation behavior of as-cast Mg−Zn−Mn−Ce alloy in compression [J]. Materials Science and Engineering A, 2013, 560: 492−499.

[4] GAO Lei, LUO A A, WANG Shi-yi, ZENG Xiao-qin. Flow behavior and hot workability of pre-extruded AZ80 magensiu alloy [J]. Magnesium Technology, 2013, 2013: 119−125.

[5] Magnesium Elektron. Elektron ZK60A forgings [EB/OL]. [2014−10−7]. http://www.magnesium-elektron.com/products-services.asp?ID=10.

[6] GALIYEV A, KAIBYSHEV R, GOTTSTEIN G. Correlation of plastic deformation and dynamic recrystallization in magnesium alloy ZK60 [J]. Acta Materialia, 2001, 49(7): 1199−1207.

[7] McQUEEN H J, MYSHLYAEV M M, MWEMBELA A. Microstructural evolution and strength in hot working of ZK60 and other Mg alloys [J]. Canadian Metallurgical Quarterly, 2003, 42(1): 97−112.

[8] WANG C Y, WANG X J, CHANG H, WU K, ZHENG M Y. Processing maps for hot working of ZK60 magnesium alloy [J]. Materials Science and Engineering A, 2007, 464(1): 52−58.

[9] SHAHZAD M, WAGNER L. Microstructure development during extrusion in a wrought Mg−Zn−Zr alloy [J]. Scripta Materialia, 2009, 60(7): 536−538.

[10] SHAHZAD M, WAGNER L. The role of Zr-rich cores in strength differential effect in an extruded Mg−Zn−Zr alloy [J]. Journal of Alloys and Compounds, 2009, 486(1): 103−108.

[11] CHEN X H, HUANG X W, PAN F S, TANG A T, WANG J F, ZHANG D F. Effects of heat treatment on microstructure and mechanical properties of ZK60 Mg alloy [J]. Transactions of Nonferrous Metals Society of China, 2011, 21(4): 754−760.

[12] AVEDESIAN M M, BAKER H. Magnesium and magnesium alloys [M]. Geauga: ASM International, 1999.

[13] SELLARS C M, MCTEGART W J. On the mechanism of hot deformation [J]. Acta Metallurgica, 1966, 14(9): 1136−1138.

[14] GAROFALO F. An empirical relation defining the stress dependence of minimum creep rate in metals [J]. Trans Metall Soc AIME, 1963, 227(2): 351−355.

[15] McQUEEN H J, RYAN N D. Constitutive analysis in hot working [J]. Materials Science and Engineering A, 2002, 322(1): 43−63.

[16] MWEMBELA A, KONOPLEVA E B, McQUEEN H J. Microstructural development in Mg alloy AZ31 during hot working [J]. Scripta Materialia, 1997, 37(11): 1789−1795.

[17] MIRZADEH H, CABRERA J M, NAJAFIZADEH A. Constitutive relationships for hot deformation of austenite [J]. Acta Materialia, 2011, 59(16): 6441−6448.

[18] WU H Y, YANG J C, LIAO J H, ZHU F J. Dynamic behavior of extruded AZ61 Mg alloy during hot compression [J]. Materials

Science and Engineering A, 2012, 535: 68−75.
[19] WATANABE H, MUKAI T, KOHZU M, TANABE S, HIGASHI K. Effect of temperature and grain size on the dominant diffusion process for superplastic flow in an AZ61 magnesium alloy [J]. Acta Materialia, 1999, 47(14): 3753−3758.
[20] COMBRONDE J, BREBEC G. Anisotropy for self diffusion in magesium [J]. Acta Metallurgca, 1971, 19: 1393−1399.
[21] SLOOFF F A, ZHOU J, DUSZCZYK J. Constitutive analysis of wrought magnesium alloy Mg−Al4−Zn1 [J]. Scripta Materialia, 2007, 57(8): 759−762.
[22] WU Y Z, YAN H G, ZHU S Q, CHEN J H, LIU A M, LIU X L. Flow behavior and microstructure of ZK60 magnesium alloy compressed at high strain rate [J]. Transactions of Nonferrous Metals Society of China, 2014, 24(4): 930−939.
[23] RAO K P, PRASAD Y, HORT N. Hot workability characteristics of cast and homogenized Mg−3Sn−1Ca alloy [J]. Journal of Materials Processing Technology, 2008, 201(1): 359−363.
[24] ZHENG X W, LUO A A, DONG J, SACHDEV A K, DING W J. Plastic flow behavior of a high-strength magnesium alloy NZ30K [J]. Materials Science and Engineering A, 2012, 532: 616−622.
[25] PRASAD Y, GEGEL H L, DORAIVELU S M, MALAS J C, MORGAN J T, LARK K A, BARKER D R. Modeling of dynamic material behavior in hot deformation: Forging of Ti-6242 [J]. Metallurgical Transactions A, 1984, 15(10): 1883−1892.
[26] RAO K P, PRASAD Y, SURESH K. Hot deformation behavior of Mg−2Sn−2Ca alloy in as-cast condition and after homogenization [J]. Materials Science and Engineering A, 2012, 552: 444−450.
[27] PRASAD Y. Recent advances in the science of mechanical processing [J]. Indian Journal of Technology, 1990, 28(6−8): 435−451.
[28] SIVAKESAVAM O, RAO I S, PRASAD Y V R K. Processing map for hot working of as cast magnesium [J]. Materials Science and Technology, 1993, 9: 805−810.
[29] EBRAHIMI G R, MALDAR A R, EBRAHIMI R. Effect of thermomechanical parameters on dynamically recrystallized grain size of AZ91 magnesium alloy [J]. Journal of Alloys and Compounds, 2011, 509(6): 2703−2708.
[30] MIRONOV S, MOTOHASHI Y, KAIBYSHEV R. Grain growth behaviors in a friction-stir-welded ZK60 magnesium alloy [J]. Materials Transactions, 2007, 48(6): 1387−1395.
[31] BEER A G, BARNETT M R. Influence of initial microstructure on the hot working flow stress of Mg−3Al−1Zn [J]. Materials Science and Engineering A, 2006, 423(1): 292−299.
[32] BARNETT M R, KESHAVARZ Z, BEER A G. Influence of grain size on the compressive deformation of wrought Mg−3Al−1Zn [J]. Acta Materialia, 2004, 52(17): 5093−5103.
[33] LÜ B J, PENG J, SHI D W. Constitutive modeling of dynamic recrystallization kinetics and processing maps of Mg−2.0Zn−0.3Zr alloy based on true stress–strain curves [J]. Materials Science and Engineering A, 2013, 560: 727−733.

挤压态 ZK60A 镁合金高温变形行为和加工性能

汪时宜[1]，高 磊[2]，Alan A. LUO[3]，李德江[1]，曾小勤[1]

1. 上海交通大学 轻合金精密成型国家工程研究中心，上海 200240；
2. 通用汽车中国研究院，上海 201206；
3. College of Engineering, the Ohio State University, Columbus, OH 43210, USA

摘 要：通过在温度为 250~450 °C 和应变速率为 0.001~10 s^{-1} 条件下进行压缩测试，研究挤压态 ZK60A 镁合金的高温变形行为和加工性能。ZK60A 镁合金的本构方程可以用双曲正弦函数进行描述。在真应变为−0.2~−0.8 下构建热加工图。在 300~400 °C 以及 0.01~0.001 s^{-1} 应变速率下，材料完全再结晶(DRX)并显示出良好的加工性能。ZK60A 镁合金高温加工，例如锻造，可以进行。在变形量大于−0.5 以及应变速率高于 0.1 s^{-1} 时，实验观察到流变失稳现象，例如局部应变集中、孪生变形、晶粒异常长大、微裂纹和切变断裂，不推荐进行加工。攀移控制的位错蠕变主导 ZK60A 镁合金的塑性变形以及动态再结晶形核。

关键词：挤压态 ZK60A 镁合金；高温变形；加工图；本构方程；加工性能

(Edited by Yun-bin HE)